

*Full Length Research Paper*

# Spatial distribution in long-wave radiation flux in São Paulo City, Brazil

Gael Clemente Jean<sup>1\*</sup> and Alfonso K. Iñárritu<sup>2</sup>

<sup>1</sup>Department of Geography, Faculty of Sciences and Technology, UNESP - São Paulo State University, Rua Roberto Simonsen, 305 19060.900 Presidente Prudente, Brazil.

<sup>2</sup>Department of Geography, Faculty of Philosophy and Humanities, USP - University of São Paulo, Avenida Prof. Lineu Prestes, 338 05508.080 São Paulo, Brazil.

Accepted December 13, 2013

The long-wave radiation ( $L^*$ ) in the urban canyons in São Paulo City, Brazil was observed through the use of a Pyrgeometer PIR model (Precision Infrared Radiometer by Eppley) and a Net Radiometer LITE model (NR-LITE by Kipp & Zonen). A simple scheme to estimate the upward longwave radiation ( $L_{\uparrow}$ ) from observations of the net all-wave radiation ( $Q^*$ ) is evaluated using a 2,200 km dataset. The instruments are set up on a mobile platform, which moves through the bottom of the canyons. The results are compared with the observed wall surface apparent temperatures. The thermal and radiation patterns are verified along the traverses through the different land use types in typical nocturnal and diurnal periods during the dry season. This upward long-wave radiation parameterization is most sensitive to urban aspect ratio effects on incoming long-wave radiation ( $L_{\downarrow}$ ). Air temperature measurements and estimates of the convective  $Q_H$  flux between the atmosphere and urban buildings are also taken. For incoming long-wave radiation, even clear sky estimates show a large degree of scatter, the results degrade as intensive vehicle traffic periods are included.

**Key words:** Surface radiation balance, urban climate, mobile measurements.

## INTRODUCTION

The main goal of this study is to demonstrate a traverse instrumental procedure works and the application of its method in urban climate studies. Long-wave emissions in the thermal infrared band are directly related to the thermal state of surfaces. In recent decades, high-precision sensors have been developed that allow patterns in both the density of the radiative flux emitted by surfaces and their apparent temperature to be detected with greater accuracy. In view of the relatively low cost of such sensors, a mobile platform was designed to observe long-wave radiative fluxes and thus obtain a

general view of their spatial distribution in the São Paulo metropolitan region (SPMR).

Mobile platforms have been little used on urban surfaces to observe spatial patterns. These platforms can be assembled with remote sensing detectors, thermometers and radiometers that are sensitive to the thermal infrared band corresponding to the atmospheric window (between 8 and 14  $\mu\text{m}$ ). The results found in the literature indicate the existence of patterns that are simultaneously the result of temporal and spatial evolution. Here we focus on spatial evolution.

In terms of studies of urban climate in the atmospheric layer closest to the surface (Stewart, 2011), mobile measurements were first used by Wilhelm Schmidt in the early 1920s in Vienna, Austria. Since the 1980s, mobile surface platforms have been ignored and replaced by

\*Corresponding author. E-mail: [gael\\_jean896@gmail.com](mailto:gael_jean896@gmail.com)

orbital platforms in an attempt to estimate the various effects associated with urban climate, such as heat islands.

However, to obtain a more realistic spatial distribution of temperatures at the various urban surfaces (Marciotto et al., 2010), the use of mobile transects on the surfaces should also be considered (Voogt and Oke, 1998; Machado and Azevedo, 2007). In general, when mobile transects are used, both the air temperature and the temperature of the walls making up the urban canyons are measured. This type of investigation can be carried out with remote sensing equipment (e.g., infrared thermometers, or IRTs) mounted on vehicles traveling along streets, roads and avenues, just as this equipment is used with orbital platforms.

The temporal and spatial variability of the temperatures of urban surfaces and the air adjacent to or above them is the result of a complex exchange of energy fluxes through a volume containing these surfaces. The fluxes can be represented by an energy balance (Offerle et al., 2006) between energy sources and sinks:

$$Q^* + Q_F = Q_H + Q_E + \Delta Q_S + \Delta Q_A \quad (1)$$

where  $Q_H$  is the convective loss in the form of sensible heat,  $Q_E$  is the convective loss of latent heat,  $\Delta Q_S$  is the spatial variation in sensible heat flux crossing the surfaces of the canyon as a result of the thermal conductivity of urban materials,  $\Delta Q_A$  represents the change in energy due to the advection of air through this volume and  $Q_F$  corresponds to anthropogenic heat sources.  $Q^*$  represents the heat received by radiative transfer and includes two components: shortwave radiation (K) and longwave radiation (L):

$$Q^* = K\downarrow - K\uparrow + L\downarrow - L\uparrow \quad (2)$$

The heat flow across an urban surface is given by:

$$G^D = \sum a_i G_i \quad (3)$$

where  $i$  represents a particular type of land cover in a given area  $a_i$  of the observed domain.

If an urban volume containing the interface between the surface and the atmosphere is defined (Ferreira et al., 2013), the term  $\Delta Q_S$  represents the variability of the energy stored in this volume and is associated primarily with the release of heat by conduction from the various materials in the volume.  $\Delta Q_A$  represents the variation in the energy advected between regions with different land cover.

The thermal patterns observed in São Paulo are complex, not only because the urban surface is complex, but also because of the different seasons in the region. The tropical climate in São Paulo changes during the year and can be clearly separated into a dry season

(April to August) and wet season (September to March). Furthermore, daily variations in temperature can be greater than the mean annual variation in temperature. Because of these characteristics, realistic estimates of the terms in the energy balance equation (Voogt and Oke, 1998) require more accurate measurements.

Temperature fields observed remotely from orbital platforms are not always adjusted to compensate for the effects of the orientation of the sensor relative to the targets on the surface (Soux et al., 2004). As a result, it is often necessary to validate the fields by comparison with surface observations. In other cases, the amount of humidity stored in surfaces must be reported (Spronken-Smith et al., 2000), particularly when urban parks are being investigated.

Oke (1987) mentions that these measuring procedures can lead to maximum errors in estimates of between 1 and 2°C when no adjustment is made. In the case of remote observations made at the surface, the atmospheric effect is reduced considerably because the targets are much closer to the sensors. In this case the main sources of error are surface emissivity estimates and the accuracy of the sensors used. In microscale experiments, precision IRTs yield more satisfactory results if the angle of view in relation to the target is smaller (Loridan et al., 2013).

When comparing the results of this study with similar studies for other cities, it should be remembered that the population of the city of São Paulo is 10,886,518 (CETESB, 2009) and that if the SPMR is included, this figure increases to 18,278,703 (CETESB, 2009). The observations reported here were made using a mobile surface platform coupled to a net radiometer (Machado, 2009; 2012). The effective emissivity investigated here indicates not only the capacity of the lower layers of the atmosphere to emit long-wave radiation toward the surface as a result of their composition and thermal stratification (Offerle et al., 2003; Bárbaro et al., 2010), but also the contributions made by building façades. In São Paulo, maximum effective emissivity occurs in September because of the low humidity content of the atmosphere (Ferreira et al., 2012).

## DESCRIPTION OF THE METHOD

### Sensors and procedures

The following sensors were used for the mobile transects:

- Pyrgeometer, model PIR (Eppley Laboratory Inc., Newport, RI, USA), sensitive to radiation in the 4.0 to 50.0  $\mu\text{m}$  spectrum, serial number 34364F3, sensitivity 3.72  $\mu\text{V W}^{-1} \text{m}^{-2}$ , hemispherical angle of view and 2 s response time.
- Micrologger, model CR3000 (Campbell Scientific Inc., Logan, USA), serial number 1189, 14 channel, supplied by two rechargeable 9 V acid batteries.

- Net radiometer, model NR-LITE (Kipp and Zonen, Delft, The Netherlands), serial number 052002, sensitivity  $13.6 \mu\text{V W}^{-1} \text{m}^{-2}$ , two sensors diametrically opposite each other, hemispherical field of view (each sensor) and an expected range of  $-200 \text{ Wm}^{-2}$  to  $1500 \text{ Wm}^{-2}$  for the resulting flux.

- Two infrared thermal sensors, model SI-431 (Apogee, Logan, USA), sensitive to the radiation in the 6.0 to 14.0  $\mu\text{m}$  spectrum, serial numbers 2061 and 2065, angle of view approximately  $20^\circ$  and response time less than 1 s.

- Temperature sensor, model RTD (RM Young, Traverse City, USA), serial number TS11223, sensitive to temperatures in the range  $-50^\circ\text{C}$  to  $+50^\circ\text{C}$ .

- Set of fifteen thermocouples, fine wire model (Campbell Scientific Inc., Logan, USA), 0.003", type T (copper-constantan), serial number 3278.

Observations were taken using a mobile platform (Figure 1) mounted on an automobile, Escort Hobby model (Ford). The vehicle was used as a mobile laboratory and had a metal support for a net radiometer. This support was attached to the front of the vehicle, while the platform with the other sensors was attached to the roof.

To avoid the measurements made with the net radiometer being affected by radiation from other vehicles and from the test vehicle itself, a non-refracting ring was installed around the radiometer. The restriction on the field of view is minimal and does not appear to affect the results. This restriction is unavoidable as the ring prevents any undesirable effects caused by thermal radiation from vehicles circulating when measurements are being taken, particularly in busy streets. In addition, the ring reduces the influence of the wind on the sensor, whether it be the natural circulation of air or artificial circulation as a result of the movement of the automobile.

All transects were georeferenced by taking simultaneous readings with a manual GPS receiver, model GPS12 (GARMIN).

The response time for all the sensors is shown in Table 1. The net radiometer and temperature sensor have a slower response time than the IRTs and pyrgeometer. This has implications for data sampling and storage intervals if the proposed experimental arrangement is to be able to detect spatial changes in fluxes associated with changes in land cover. Because of this a sampling frequency of 0.5 Hz and storage frequency of 0.1 Hz were stipulated.

An average vehicle speed of about  $30 \text{ kmh}^{-1}$  was considered reasonable, and the vehicle was kept to the right of the road whenever possible, in accordance with the Brazilian Highway Code. The need to travel at higher speeds on some major roads to avoid causing problems for other drivers nearby meant that there was some loss in spatial resolution.

### Transects and sampling points

The spatial variability of  $L\downarrow$  can be analyzed by considering

considering different types of land use. The results are presented here in terms of four of such types of land use: a) central, densely built up with very clear presence of vertical surfaces; b) garden city, with a large number of trees; c) expressways, with a significant reduction in form factor together with the presence of warehouses and very large roofs; and d) residential, with a mixture of commercial and residential land use, as well as major changes in all the elements of urban form. These areas are distributed inside the polygon represented by the clear white line in Figure 2, which represents quite accurately the physical limits beyond which the effects of urbanization become gradually less noticeable.

### Estimating $L^*$

Previous experiments have shown that the methodology proposed here is able to detect the fundamental effects associated with urban climate, such as heat islands and variations in the temperature of canyon walls (Machado and Azevedo, 2007). However, in terms of the spatial detailing of long waves, the net longwave radiation ( $L^*$ ) is yet to be determined. To do this, the flux  $L\uparrow$ , which is not measured directly in the proposed method, must be specified:

$$L^* = L\downarrow - L\uparrow . \quad (4)$$

During the night, the upwelling long-wave component can easily be obtained from  $Q^*$  and  $L\downarrow$ :

$$L\uparrow = L\downarrow - Q^* \quad (5)$$

During the day, however, the above procedure is not appropriate as the radiation balance equation must also take net short waves ( $K^*$ ) into consideration. As these waves were not observed specifically, a parameterization proposed in a preliminary study is used (Offerle et al., 2003).

The parameterization for the upwelling long-wave flux in (Offerle et al., 2003) can be rewritten as:

$$L\uparrow = \varepsilon_0 \sigma T_a^4 + 0.08 K^* + (1 - \varepsilon_0) L\downarrow . \quad (6)$$

As

$$Q^* = K^* + L^* , \quad (7)$$

Substituting equation (7) in (6) and expanding  $L^*$  in terms of the components emitted and received by the surface gives a new form of the parameterization proposed by Offerle et al. (2003):

$$L\uparrow = 1.087 \varepsilon_0 \sigma T_a^4 + 0.087 Q^* + (1 - 1.087 \varepsilon_0) L\downarrow . \quad (8)$$

### Calculating sensible heat flux $Q_H$

Some fluxes from urban surfaces are associated with

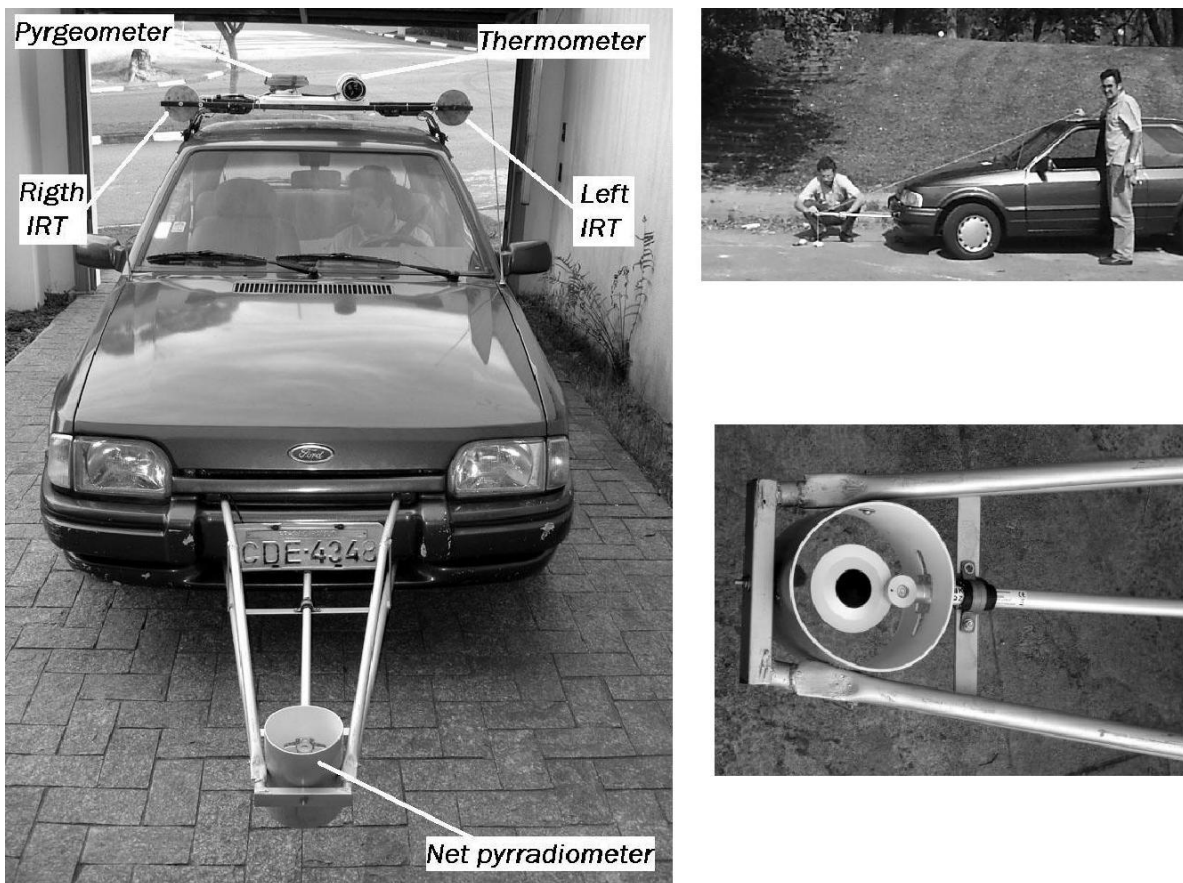


**Figure 1.** The mobile platform (left), with the net-radiometer fixed to the front of the vehicle. The viewing angle (right, above) and detail of the net-radiometer (right, below).

**Table 1.** Response time (seconds) of all instruments used.

Parameter	Response time (s)	Ambient temperature (°C)
Net radiometer	< 20	- 30 to + 70
Pyrgometer	2	- 20 to + 40
IRTs	< 1	- 30 to + 65
Air temperature	10	- 50 to + 50

turbulent energy or convective exchanges. They are directly associated with the physical properties of the atmosphere, such as air temperature ( $T_a$ ), density ( $\rho$ ) and constant pressure specific heat ( $c_p$ ), as well as the properties of the surface, such as its temperature ( $T_s$ ).

These fluxes have generally been investigated and described in terms of their mathematical representations and integrated over a variety of surfaces. Unlike net radiation ( $Q^*$ ), which is observed, and anthropogenic heat (QF), which is determined from an inventory of various sources, sensible heat flux (QH) can be expressed (Hu et al., 1999) as follows:

$$QH = \sum a_i \rho c_p (T_s - T_a) \tag{9}$$

where  $c_p$  and  $\rho$  for the city of São Paulo are in the region of  $10^{-3} \text{ J.kg}^{-1}.\text{C}^{-1}$  and  $925 \text{ g.m}^{-3}$ , respectively. By applying equation (9) for the temperatures observed during the mobile transects, the sensible heat flux between the urban atmosphere and canyon walls can be estimated.

### URBAN TRANSECTS AND OTHER EXPERIMENTS

Between July 27<sup>th</sup>, 2006, and November 13<sup>th</sup>, 2007 (a period of one year and four months), forty-three

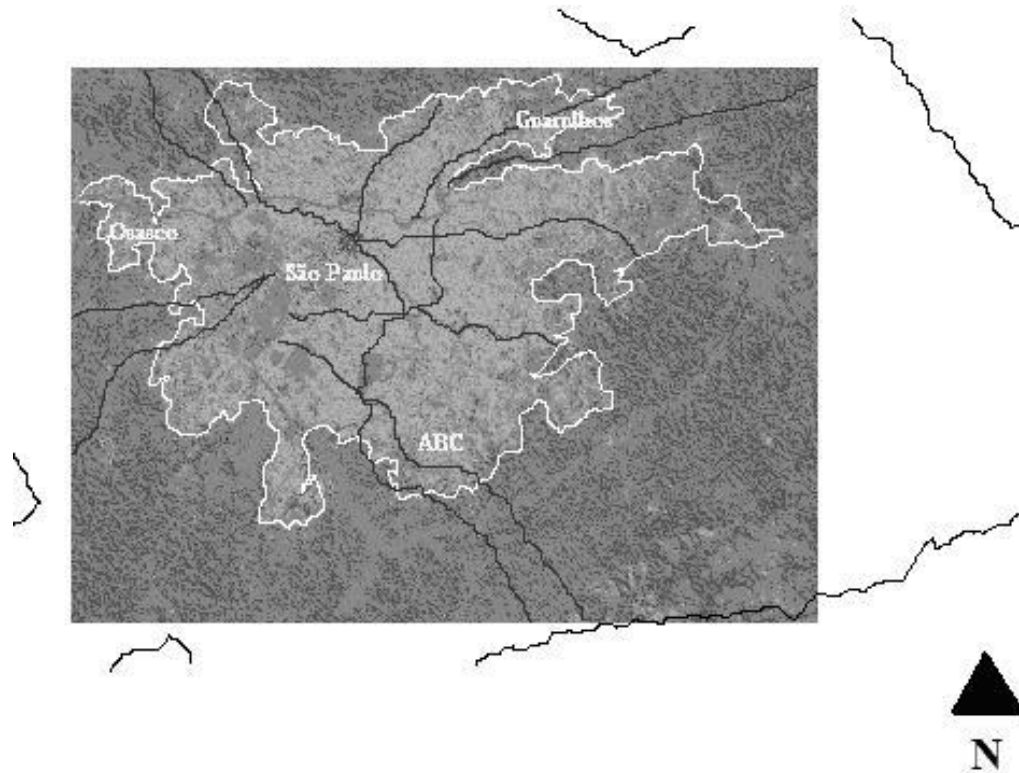


**Figure 2.** Road network that makes up the sampling transects (dark lines), arranged on a image of the estimated  $Q^*$  flux. The polygon represented by the white line corresponds to the boundary between the MRSP area considered urbanized (inside) and the peripheral area in which the urban features are attenuated to the regional features (outside).

**Table 2.** Summary of the data collected.

| Observation period<br>(year/ year day) |
|----------------------------------------|----------------------------------------|----------------------------------------|----------------------------------------|
| ME 2006/ 208                           | ME 2006/ 216                           | ME 2006/ 223                           | ME 2006/ 230                           |
| ME 2006/ 237                           | ME 2006/ 251                           | ME 2006/ 354                           | ME 2006/ 364                           |
| ME 2007/ 011                           | ME 2007/ 025                           | ME 2007/ 038                           | ME 2007/ 047                           |
| ME 2007/ 060                           | FE 2007/ 081                           | PE 2007/ 090                           | ME 2007/ 102                           |
| ME 2007/ 112                           | ME 2007/ 121                           | ME 2007/ 132                           | ME 2007/ 141                           |
| ME 2007/ 151                           | ME 2007/ 161                           | FE 2007/ 179                           | PE 2007/ 188                           |
| ME 2007/ 195                           | ME 2007/ 203                           | ME 2007/ 210                           | ME 2007/ 212                           |
| ME 2007/ 216                           | ME 2007/ 219                           | ME 2007/ 220                           | ME 2007/ 223                           |
| ME 2007/ 225                           | ME 2007/ 227                           | FE 2007/ 235                           | FE 2007/ 238                           |
| PE 2007/ 239                           | PE 2007/ 246                           | ME 2007/ 255                           | EM 2007/ 261                           |
| ME 2007/ 283                           | ME 2007/ 294                           | ME 2007/ 317                           |                                        |

experiments were carried out (Table 2), of which thirty-five were mobile (ME), four fixed (FE) and four photographic (PE).

#### Fixed observations

Fixed observations were made during the fall and winter

of 2007 in *Rua Sebastião Cortes* in the *Perdizes* neighborhood along a simple wedge-shaped traverse starting and finishing in *Rua Campevas*, near *Avenida Sumaré* in the west of the city of São Paulo. The following elements of the urban surface were investigated: trees, walls, asphalt cover and the air close to the surface. The hourly variability resulting from different exposure to the

sky and different amounts of shade provided by trees was observed. The micrologger temperature was used as a reference for measurements made with the thermocouples. Unlike in the autumn, the street is completely overshadowed by buildings in the afternoon. Although there is considerably less human activity in this area than in adjacent areas, such as *Avenida Sumaré*, pedestrians and vehicles were observed circulating in the area.

## DEMONSTRATION OF THE METHOD

### Urban sprawl

Table 3 shows the twenty-seven most frequently visited locations among those visited in the period up to November 2007. Frequency in this context means the number of days when the authors were in a specific location during the one-and-a-half-year period in which measurements were taken. Many other locations covering a wide range of land uses were also visited, but because of their large number they could not be included in a single table. Some locations were visited more frequently simply for logistical reasons.

### Metropolitan region

An approximate representation of the network of transects covered by the mobile laboratory that could be successfully and continuously georeferenced is shown in Figure 3. This network was specified in terms of astronomical coordinates and the geopolitical limits of the city of São Paulo. It can be seen that some of the transects extend beyond these limits, indicating that the investigation in fact, extended to parts of the SPMR.

## SPECIFIC TRANSECTS

Figure 4 shows data collected from a transect approximately 2.6 km long extending along *Avenida Cerro Corá* and *Avenida Heitor Penteado* from the intersection with *Avenida São Gualter* to the intersection with *Avenida Pompéia*. This specific experiment illustrates how the investigations were carried out across the SPMR and also helps to show clarify details related to data storage. During the initial experiments one averaged data item was recorded every 60 s. Subsequently, it was agreed to reduce this minimum storage interval to 10 s in order to achieve greater spatial detail while at the same time taking into account the maximum response time for the sensors being used.

The specific transect described in this here was performed on three different occasions. The first was on Friday February 16<sup>th</sup>, 2007, between 2:40 pm and 2:55 pm, when the weather was sunny with a few clouds. There was more traffic than usual because it was the day before the long Carnival public holiday. The second occasion was on Thursday March 1<sup>st</sup>, 2007, between

2:01 pm and 2:11 pm, when the weather was sunny with barely any clouds. Although it was a normal working day, the traffic was not very heavy. The third occasion was Monday May 21<sup>st</sup>, 2007, between 6:43 am and 6:52 am, when the sky was starry with occasional scattered clouds. The traffic was light, as usual after a weekend.

### Metropolitan region

After the radiative fluxes had been acquired, the next step was to organize them. The key feature of the database was that the statistical data were separated into four different files: mean values for the 10 s interval, standard deviation and maximum and minimum values for the same interval. The data were organized this way because of the programming used in the micrologger. To analyze the data, an auxiliary program was developed that mixed the data acquired with the micrologger with the coordinates acquired using the GPS receiver. This program, which was compiled satisfactorily for all the experiments carried out, essentially performs a linear interpolation of the acquired coordinates (C) for the locations georeferenced during the experiments:

$$C(t) = C_0 + (t - t_0) \frac{\partial C}{\partial t} \quad , \quad (10)$$

where  $t$  is the instant at which the mean temperature or radiation was recorded and stored in the micrologger and  $t_0$  is the most recent instant before that when a GPS reference coordinate ( $C_0$ ) was acquired by the GPS system.

The variability observed for the data suggests that it has a well-defined frequency distribution (Figure 5) with the characteristics of a normal distribution. The air temperature observed in the SPMR, for all experiments carried out, ranged between a maximum of 36°C and a minimum slightly above 8°C.

The sampled data for the air temperature and the temperature of the ring around the net radiometer suggest that these have quite similar distributions. This would indicate that there is a thermal equilibrium between the ring and the air flow over the device.

### Variability of Q\*

To demonstrate the variability of Q\*, we used two different transects, both georeferenced and performed during the summer of 2006/2007. The first transect covered the *Anhangüera* highway from the vicinity of the *Perus* intersection, through *Vila Jaguará* as far as the *Marginal dos Pinheiros* and along the *Marginal dos Pinheiros* to *Ari Torres* bridge. It was conducted on Saturday December 30<sup>th</sup>, in the early morning, during a long weekend. Mean speed was approximately 30 kmh<sup>-1</sup>. The sky was clear and the weather calm. The second

**Table 3.** Distribution of the main sampled site visited more one time (frequency).

Site	Freq.								
ABC	2	A.Paulista	5	G.Acarolina	3	Pt.Piqueri	7	R.Cantareira	2
Al.Nothmann	2	A.PedAlvCabr	2	J.Gloria	2	Pt.Pompeia	3	R.CapoteVale	2
A.AlcantMach	2	A.Pompeia	3	L.Arouche	2	Pt.Tatuape	3	R.CardealArc	2
A.AssisRibeir	2	A.QueirozFilh	2	L.Batata	2	Pt.Transamer	2	R.CardAlmeid	2
A.Bandeirant	3	A.RadialLest	2	L.SaoFrancis	2	PçBuenAires	2	R.Clelia	4
A.Brasil	2	A.Reboucas	3	M.Pinheiros	9	PçCharMuller	2	R.Coriolano	4
A.BrasLeme	2	A.RioBranco	2	M.Tiete	16	PçJoaoMend	3	R.CunhaGago	2
A.Brig.FarLim	6	A.Rudge	2	Mun.EmbuArt	2	PçPanameric	6	R.Dardanelos	35
A.Brig.LuisAn	2	A.SalimFMal	2	Mun.Guarulh	3	PçdoPatriarc	2	R.DMoraes	2
A.CerroCora	7	A.SaoGualter	15	Mun.Itaquaq	2	PçdaSe	2	R.GastaoMes	2
A.Consolacao	2	A.SaoJoao	3	Mun.Mairipor	4	PçVilaboim	2	R.Guaicurus	2
A.CorifeuAM	2	A.Sumare	5	Mun.St.Andre	2	PrefeitSPaulo	2	R.Iperoig	4
A.Diogenes	33	A.23deMaio	2	Mun.SBernar	2	Rep.Mairipor	2	R.JoaoRamal	3
A.DrArnaldo	3	A.VitalBrazil	2	Mun.SCaetan	2	Rodoanel	3	R.LiberoBada	2
A.DuqCaxias	2	B.Cambuci	2	Mun.TaboaS	4	Rod.Anchieta	2	R.Marq.S.Vic	11
A.ErmanoMar	4	B.CityLapa	7	P.AgBranca	4	Rod.Anhang	5	R.NSdaLapa	10
A.Estado	5	B.Higienopol	2	P.Ibirapuera	2	Rod.AyrtSenn	3	R.PedrosoMo	13
A.FMatarazzo	6	B.S.Mateus	2	P.VilaLobos	3	Rod.CasteloB	2	R.PioXI	30
A.FranMorato	3	B.SMiguelPta	2	Pt.Bresser	2	Rod.EmbuCot	2	R.Piracuama	4
A.HPentead	5	B.VilaMadale	2	Pt.CasaVerde	4	Rod.FernDias	4	R.StaRosa	2
A.HenrSchau	4	B.VilaMatilde	2	Pt.Cebolao	2	Rod.Mair.FrR	2	R.SenQueir	4
A.Ipiranga	5	CampusCidU	2	Pt.CidUnivers	4	Rod.PrDutra	3	R.Tito	14
A.Itaquera	2	Cem. Lapa	5	Pt.EusebioM	3	Rod.RapTav	3	R.Vergueiro	5
A.Jabaquara	2	CETESB	7	Pt.Goldfaber	2	Rod.RegisBit	3	Tr.Dard.PioXI	6
A.Mercurio	2	Col.Mackenz	2	Pt. Jaguaré	3	Rod.Roseira	2	Trev.Perus	2
A.MiguelStef	2	Elev.CosSil	4	Pt.Lapa	11	R.Apinages	3	T.MataFria	2
A.NacoUni	2	ExpTirad	2	Pt.Limao	2	R.ArturAzeve	2	Zona Cereal	3
A.Pacaambu	4	FAAP	2	Pt.Pacaambu	2	R.Butantã	3	Zona Leste	3

It can be recognized boulevards (Al), avenues (A), neighborhoods (B), cemeteries (Cem), schools (Col), highs (Elev), stadiums, (Est), casts (Exp), slums (Fav), garages (G), hospitals (Hosp), gardens (J), wides (L), marginals (M), municipalities (Mun), parks (P), bridges and overpasses (Pt), garden parks (Pç), highways (Rod), streets (R), shopping centers (Shop), lanes (Tr), interchanges (Trev), tunnels (T) and some notable localities (Company of Environmental Sanitation Technology of the State of São Paulo - CETESB).

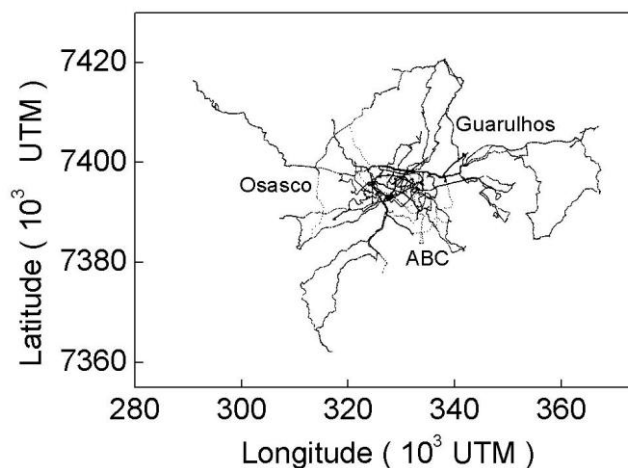


**Figure 3.** All georeferenced traverses (dotted lines) performed from July, 27 2006 and November, 30 2007 in the São Paulo Metropolitan Region (SPMR).

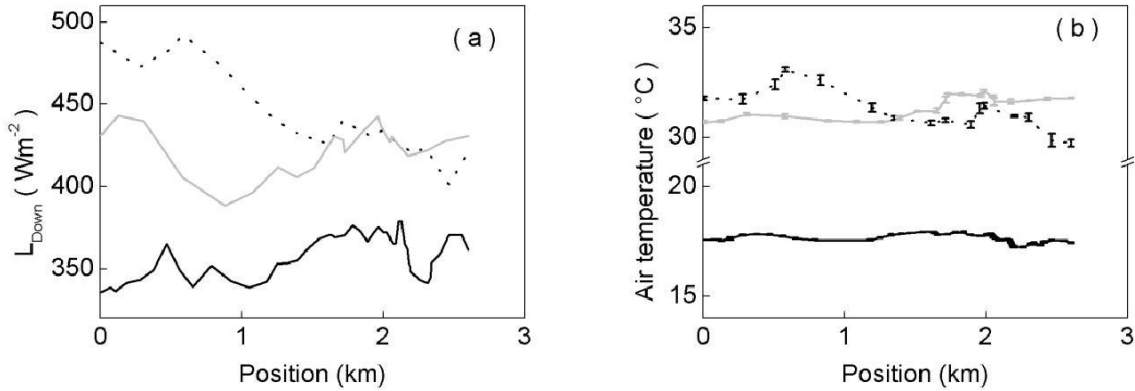


**Figure 4.** Spatial distribution of  $L_{\downarrow}$  flux (a) and air temperature (b) through Cerro Corá and Heitor Penteado Avenues, from São Gualter Avenue to the cross with Pompéia Avenue, in May, 21 (dark continuous lines), in March, 1 (light continuous lines) and in February, 16, 2007 (dotted lines). Also it is represented the observed deviation (vertical bars) to the temperature.

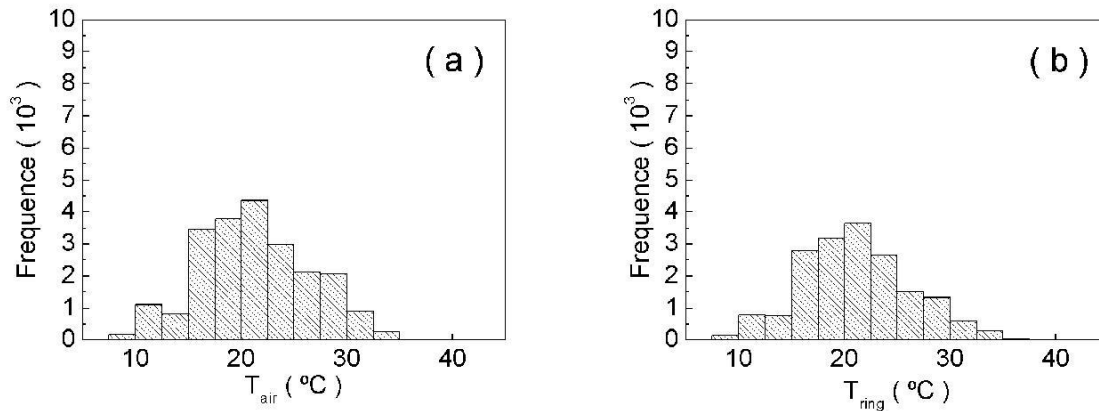


**Figure 5.** Histograms of the sampled magnitude of air temperature (a) and radiometer ring temperature (b).

transect had the same duration as the first (approximately 50 min) and covered an area between the western and central zones of the city starting in the vicinity of the *Lapa* and *Água Branca* neighborhoods and extending along *Avenida Cardoso de Almeida* to the vicinity of the *Higienópolis* and *Santa Cecília* neighborhoods. This route was covered during the afternoon of Wednesday February 7<sup>th</sup>, a typical working day. Mean speed was approximately  $10 \text{ kmh}^{-1}$ , less than in the first transect.

The sky was sunny with some scattered cumulus congestus clouds and a light wind (Figure 6). The humidity was not recorded but subjective assessments at the time suggest the experiment took place in unsaturated conditions. No fog was recorded during either experiment, but there was heavy rain after the second one.

Different patterns of  $Q^*$  were observed during the two experiments. In the first, the maximum amplitude was quite low, at  $50 \text{ Wm}^{-2}$ , while during the second it was

much higher, at around  $500 \text{ Wm}^{-2}$ . The two time series were interpolated with the simultaneous georeferencing so that the spatial distribution of  $Q^*$  along the routes could be represented graphically (Figure 7).

Although the first experiment took place in the early morning, the pattern observed was characteristic of nighttime, as from a meteorological point of view, negative  $Q^*$  values should only be observed at night. This pattern was reinforced by the presence of orographic barriers to the north of the *Tietê* river and subsequently by the presence of urban areas with intense vertical growth along the east bank of the *Pinheiros* river. In the final analysis, obstacles, whether natural or anthropogenic, determine the time at which the sun rises from the point of view of an observer traveling inside a canyon.

Intermittent oscillations of  $Q^*$  were observed (Figure 2a), particularly along the section between the *Anhangüera* highway and the *Marginal dos Pinheiros*,

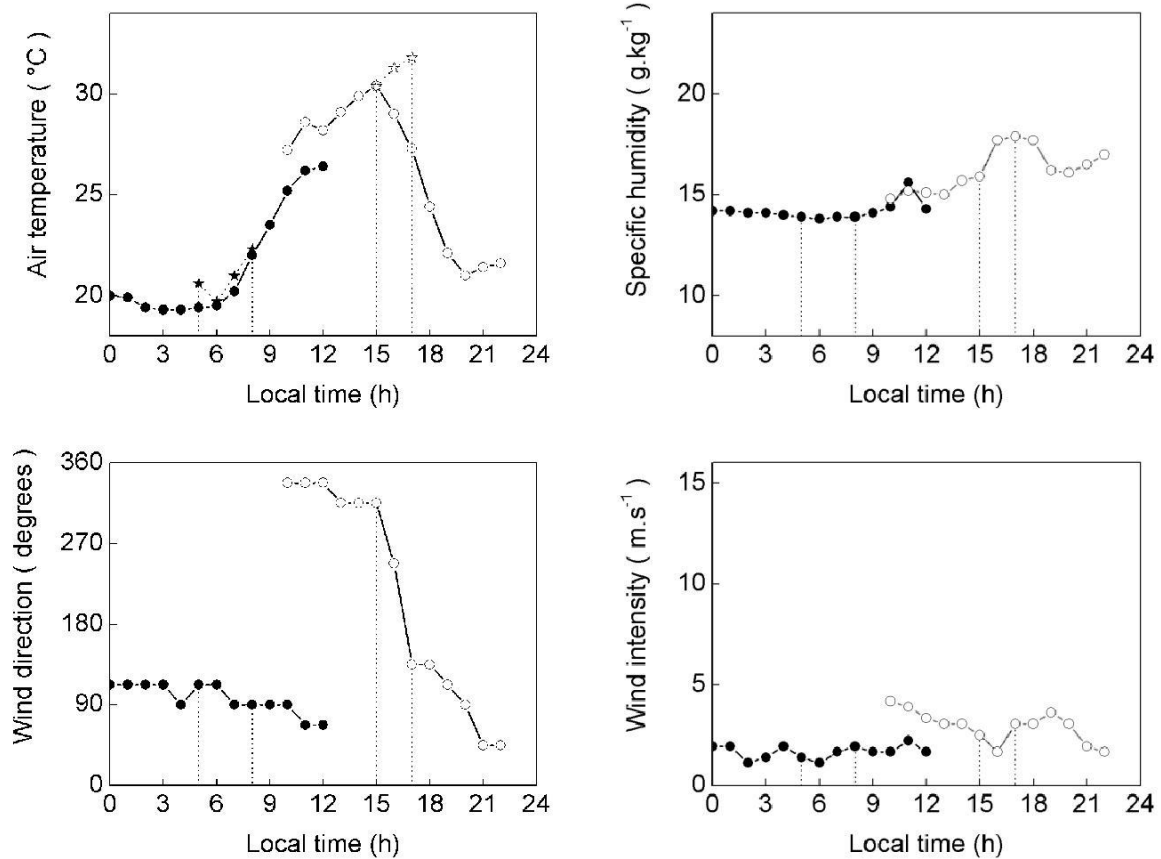


**Figure 6.** Hourly evolution of air temperature (above, left), specific humidity (above, right), wind direction (below, left) and intensity (below, right) near the surface, in December, 30 (dark circles) and in February, 7 (light circles), for a meteorological station located in the south region of the city of São Paulo and for the vehicle in displacement through the streets (stars), during a period of 12 hours around the intervals (vertical dotted lines) of the mobile experiments.

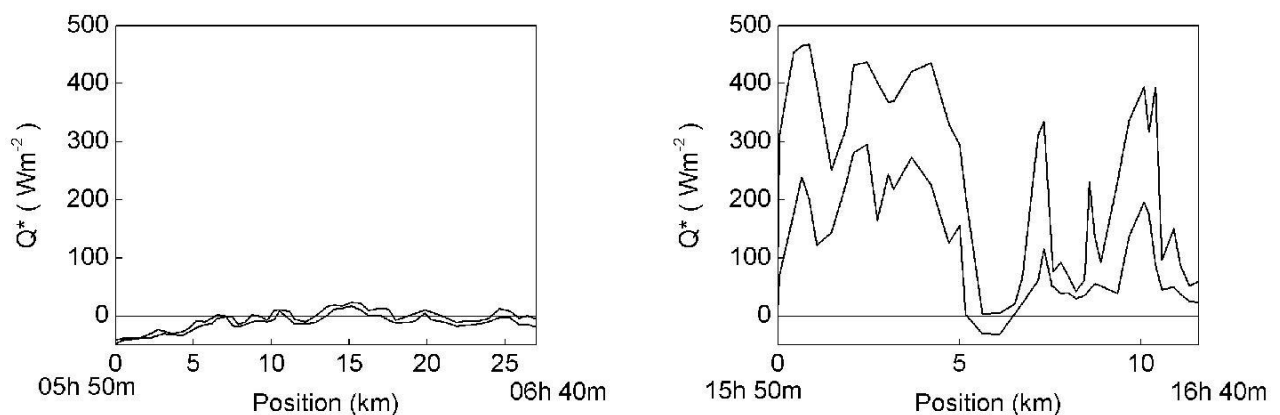


**Figure 7.** Spatil distribution of the maximum (above) and minimum (below) absolute net all-wave radiation observed through the axis Anhangüera – Marginal Pinheiros (left) and through the axis Francisco Matarazzo – Pacaembu – Higienópolis (right).

which is characterized by a transition from a widely forested area to an area where land use is typically

urban. Gradually the flux  $Q^*$  starts a transition to predominantly positive values, indicating an increase in

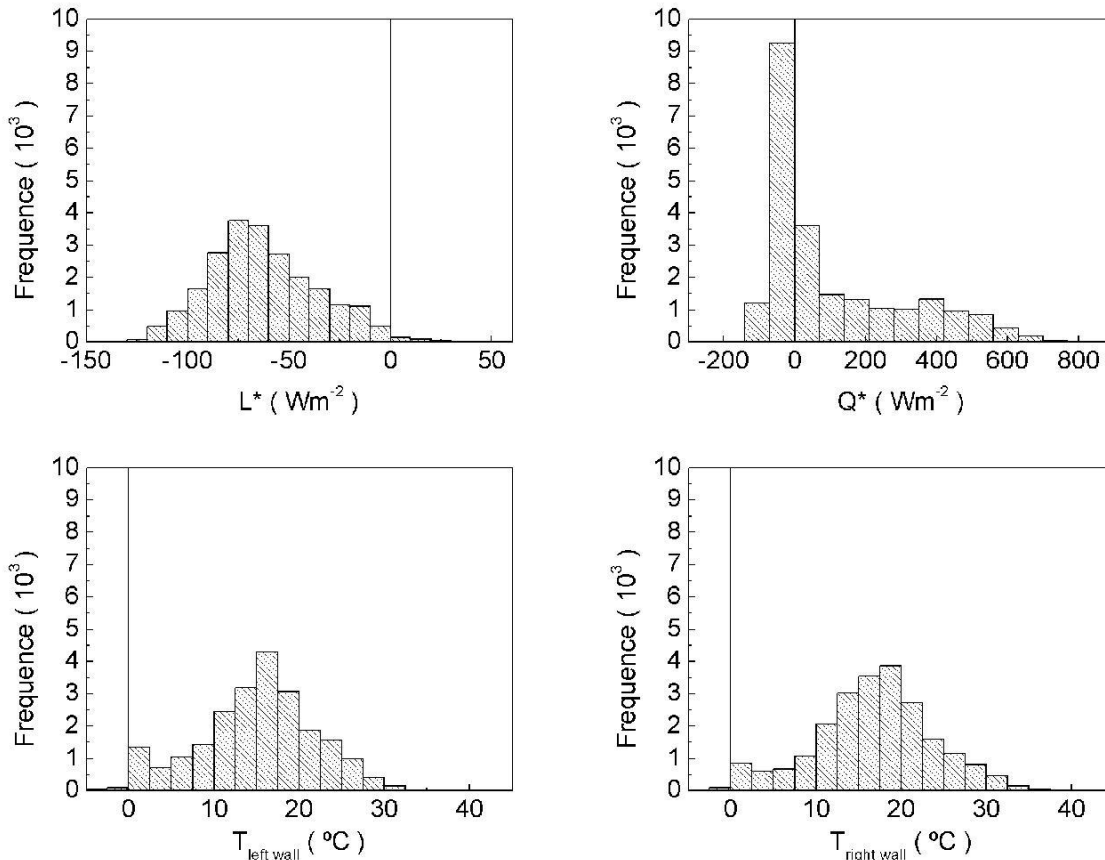


**Figure 8.** Histograms of the sampled magnitudes of the net long wave radiation over the vehicle (above, left), net all-wave radiation over the asphalt (above, right), apparent temperature on the left vertical surfaces (below, left) and apparent temperature on the right vertical surfaces (below, right).

the radiative component from the sky if it is assumed that the component emitted by the surface at the bottom of the canyon remains practically constant as a result of the uniform asphalt cover on the roads and the low thermal variability of the road surface expected while the observations were being made.

In contrast, the second experiment, which was carried out on a typical summer afternoon with the same weather conditions as the first experiment (clear sky and calm weather) revealed a pattern of  $Q^*$  that was typical of daytime, with positive values. However, some sudden reductions in  $Q^*$  were observed, and negative values series combining all the transects (a total of 2,200 km) performed in the SPMR during the experiments. The observed variability suggests that, with the exception of  $Q^*$ , the frequencies (Figure 8) have a normal distribution.

If the surface of the dome of the pyrgeometer and the air circulating around it are assumed to be in thermal equilibrium when the transects are conducted, the net long-wave radiation at a certain distance above the asphalt ( $L_N^*$ ) can then be estimated based on the observations. This distance is approximately 1.5 m above the ground and corresponds to the roof of the vehicle,

were recorded even during the day (Figure 7). These coincided with the presence of urban land cover such as flyovers, highlighting the ability of the proposed method to identify spatial variations in radiative fluxes in the presence of interference from different types of land use.

**Application of the method to determine the variability of long-wave fluxes**

The complete set of radiative fluxes and temperatures observed from the mobile platform corresponds to a time

where the mobile platform was attached. It should be noted that  $L_N^*$  is essentially negative, indicating that the base of the canyon is generally hotter than the combination of sky and building façades. The results indicate that the modal value of the magnitude of this flux is in the region of  $7 \text{ Wm}^{-2}$ .

In contrast,  $Q^*$  has positive values associated with maximum observed variations considerably greater than those for  $L_N^*$ . Although the negative values observed for  $Q^*$  are much smaller than the positive values, it can be seen that they are of the same order of magnitude as the

variations in  $L_N^*$ , as both measurements, although independent, are approximately the same during the night or when the urban cover causes an obstruction.

Although elevated maximum values associated with periods of high-intensity radiative flux were observed, it can be seen that the modal value of the distribution of  $Q^*$  is negative and has a magnitude of only  $30 \text{ Wm}^{-2}$ . This would appear to indicate that  $Q^*$  acts more as an energy sink for the system than as an energy source. Analysis of the data also showed that the temperature observed in the SPMR, when all the surfaces were taken into consideration, always stayed within the range 8 to  $36^\circ\text{C}$ .

### Estimating $L\uparrow$ and $L_W$ based on observations of $Q^*$ and façade temperatures

It is possible to make a more realistic estimate of long-wave flux in an urban environment. However, the effective value of  $L^*$  must first be estimated very close to the bottom of the canyon, at the height at which observations with the net radiometer are made (approximately 0.3 m from the surface). The first stage is to estimate the flux  $L\downarrow^1$  for this level. This is done by using the observed values of  $L^*$  and, based on the Stefan Boltzmann law for a black body, as well as on observations of air temperature, subtracting the output of the thermopile from  $L^*$ . There is assumed to be thermal equilibrium between the sensor and the air.

Having estimated  $L\downarrow$ , the component  $L\uparrow$  can also be estimated using the observed  $Q^*$ , the air temperature and the parameterization proposed for this component (Equation 8). In this case, a value of 0.95 is used for the emissivity of asphalt (Oke, 1987).

The difference between the two estimated components therefore gives an estimate of  $L^*$  very close to the asphalt cover. It should be noted that the distribution discussed above for  $L_N^*$  is very similar to that observed for  $L^*$ . One difference is that the modal value of  $L^*$  is slightly higher (approximately  $75 \text{ Wm}^{-2}$ ), perhaps because the asphalt cover is usually hotter than the air. The modal values identified for the components  $L\downarrow$  and  $L\uparrow$  are approximately 350 and  $415 \text{ Wm}^{-2}$ , respectively, indicating that in most situations the bottom of the canyon may in principle be hotter than the sky and vertical surfaces.

Similarly, the emissions from vertical surfaces ( $L_W$ ) can be estimated from the observations made with the two IRTs located on the right and left of the vehicle (Figure 9). Applying once again the Stefan-Boltzmann law for a gray body to each of the observed apparent temperature values for the walls and assuming a homogeneous emissivity of 0.9 for all the lateral targets (Oke, 1987) gives modal values of  $370 \text{ Wm}^{-2}$  and  $350 \text{ Wm}^{-2}$  for the targets on the right and left, respectively. However, it

should be borne in mind that the materials making up these targets vary greatly.

After these fundamental assumptions have been drawn up, the emissivities used for the estimates for  $L\uparrow$  and  $L_W$  can be checked. Because these estimates were arrived at using generic values for the ground and walls, whose surfaces are in fact made up of a wide variety of materials (concrete, stone, bricks, wood, glass and metal), and because there are a large number of pedestrians in some streets, the frequency distribution of the apparent temperatures observed during the fixed experiments (Figure 10) must be analyzed.

It can be seen that modal values for the asphalt and walls of approximately  $22.5$  and  $23^\circ\text{C}$ , respectively, were recorded. Although the observed temperature range for the asphalt was greater than for the walls ( $20$  and  $15^\circ\text{C}$ , respectively), this result would appear to indicate that the bottom of the canyons frequently remain overshadowed by the walls, which receive solar radiation directly.

### Estimating emissivity

Applying the Stefan-Boltzmann law for a gray body to the observed temperatures and the estimated long-wave fluxes gives the following estimates for the emissivity of asphalt and walls in the SPMR:

$$\varepsilon = \frac{L\uparrow}{\sigma T^4}, \quad (11)$$

where  $\varepsilon$  is the estimated emissivity based on observations,  $L\uparrow$  is the estimated flux of long waves emitted by surfaces,  $\sigma$  is the Stefan-Boltzmann constant and  $T$  is the observed apparent temperature.

The observed emissivity for the streets of São Paulo, which are generally covered with asphalt but occasionally with concrete (e.g., the *Rodoanel*, or orbital highway), was approximately 0.96 (Table 4). The corresponding figure for the walls, which are made from a wide variety of materials, was approximately 0.84.

The difference between the observed emissivity of the canyon floor and the emissivity used to calculate  $L^*$  near the ground suggests that the latter was underestimated by around 1%. Similarly, the emissivity of the walls was overestimated by around 7%. The great variety of materials used in walls undoubtedly influences this result, as by using an emissivity of 0.9 (concrete), the estimate is limited to its upper threshold. The literature (Krayenhoff, 2013; Oke, 1987) acknowledges that the emissivity of walls varies greatly and that the minimum value usually oscillates between 0.86 and 0.88. If values of this magnitude had been used to estimate  $L_W$ , the relative error would have been smaller.

The reduced values of  $\varepsilon$  for canyon walls reflect the low emissivity of some of the materials used in the surfaces of building façades (e.g., glass), but are also in part due

<sup>1</sup> Indeed, this component of the flux was observed directly in the initial experiments and corresponded to the first channel in the pyrgeometer. However, battery consumption for this channel proved to be quite high, and this method was not considered as precise as reading  $L^*$  directly.

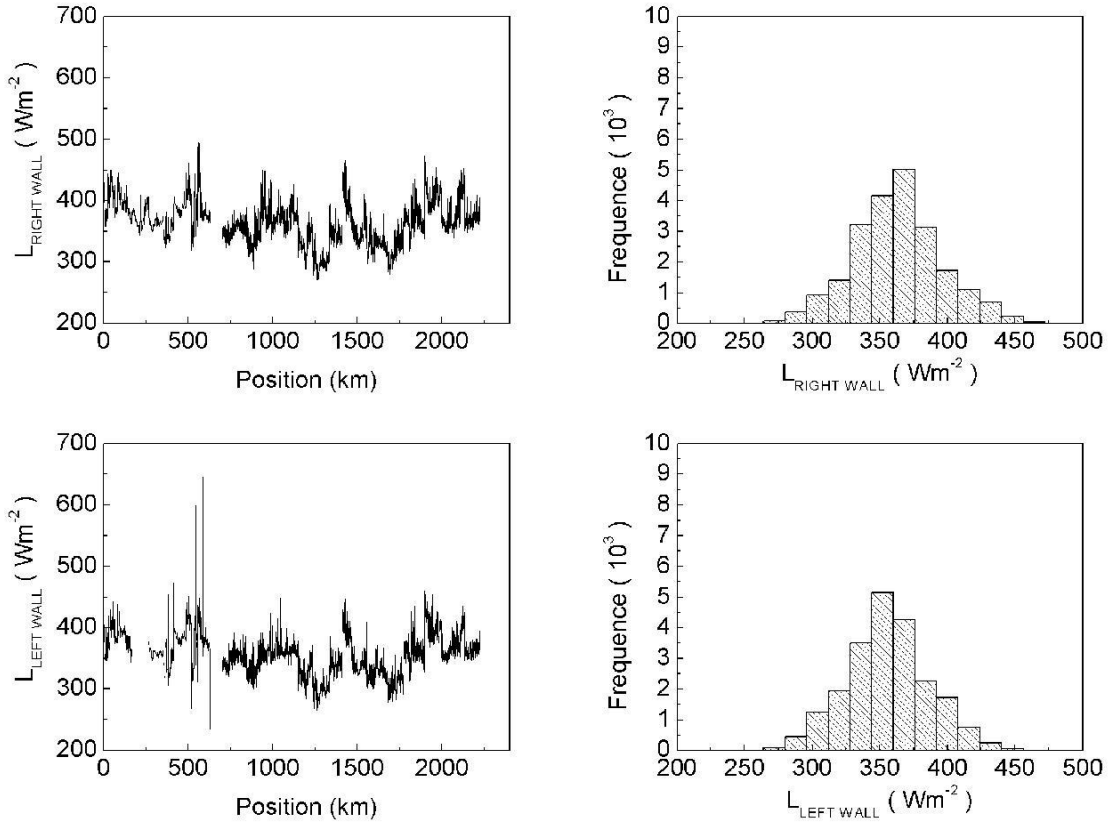


**Figure 9.** Spatial variability of the estimated longwave radiation emitted from the right walls and their amostral frequency (above), and the same to the left walls (below).

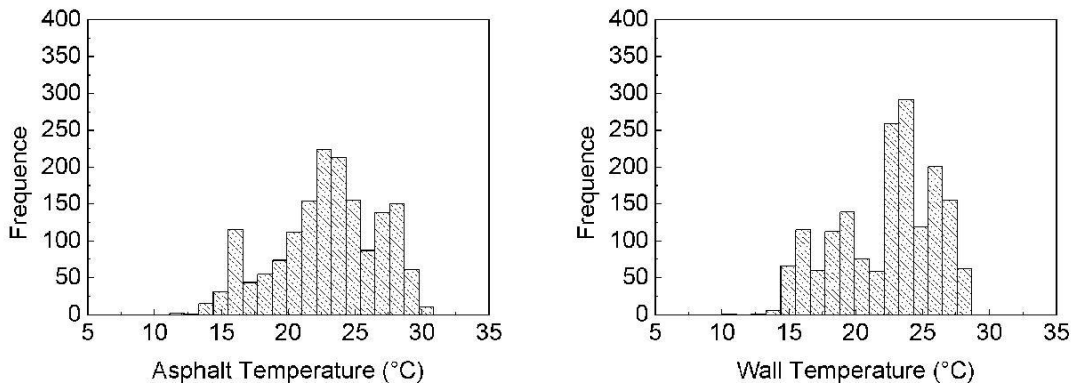


**Figure 10.** Histograms of the sampled asphaltic cover (left) and wall (right) surfaces temperatures, as recorded in Sebastião Cortês street, west zone of São Paulo.

to the fact that the observed target is very often a mixture of sky and built surface.

**ANALYSIS ON A LOCAL SCALE**

**Complete thermal characterization**

As pedestrians move around urban areas, different

energy exchanges take place between them and the surfaces that make up these areas. These energy exchanges are the result not only of the action of short waves during the day, particularly clear days, but also the constant action of long waves emitted by all the surfaces that make up the urban environment.

The contribution made by long waves has considerable spatial variability, both horizontally and vertically. Urban

**Table 4.** Estimated and observed emissivities.

Surface	Modal observed flux ( $L_{\uparrow}$ )	Modal observed temperature	Estimated emissivity [25; 27]	Observed emissivity	Estimated relative error
Asphalt	$415 \text{ Wm}^{-2}$ ( $L_{\uparrow}$ )	$22.5^{\circ}\text{C}$	0.95	0.96	- 1 %
Walls	$370 \text{ Wm}^{-2}$ ( $L_w$ )	$23.5^{\circ}\text{C}$	0.90	0.84	+ 7 %

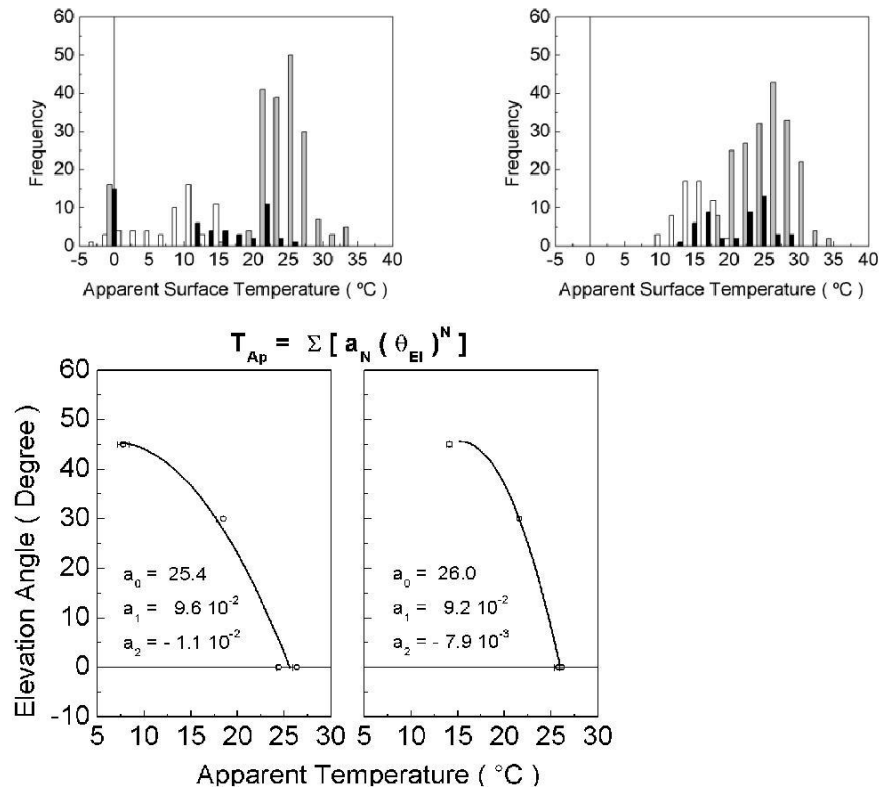


**Figure 11.** Sampling distribution of the apparent temperature of the canyon walls obtained with the IRTs sensors positioned to the right (above, right) and to the left (above, left). The gray columns indicate the sensor positioned at an elevation angle of  $0^{\circ}$ , the blacks at an angle of  $30^{\circ}$  and the whites at an angle of  $45^{\circ}$ . Vertical distribution of the mean apparent temperature (below), the bars indicate the relative error and the continuous lines suggest a second-order polynomial that best represents this distribution.

radiative emissions are anisotropic, and this becomes quite apparent when mobile observations that include observations of urban canyon walls are made (Voogt and Oke, 1998; Machado and Azevedo, 2007). In urban areas in a metropolis, the sky view factor is frequently reduced and sometimes obstructed exactly in the zenith direction (Oke, 1987, p. 355).

The difference between the temperatures of opposite walls in relation to the air temperature varies along the street (Figures 11 and 12) and is a result of the orientation of the canyon and the thermal properties of the materials, which modulate this difference. Patterns were also observed in the apparent temperature of the

asphalt cover at the bottom of the canyon (Figure 13) in the direction in which the vehicle was traveling.

Because of the relatively short duration of each experiment, the mobile observations in this study were not corrected for any temperature variations that might have been caused by a change in the position of the sun, as such variations were considered to be much less significant than those caused by changes in land cover. Examples of this are the experiments carried out in *Avenida Paulista* and *Avenida Pompéia*.

Greater temperature differences between the air and walls were observed when the sensors were rotated so as to increase their angle of elevation. This implies that

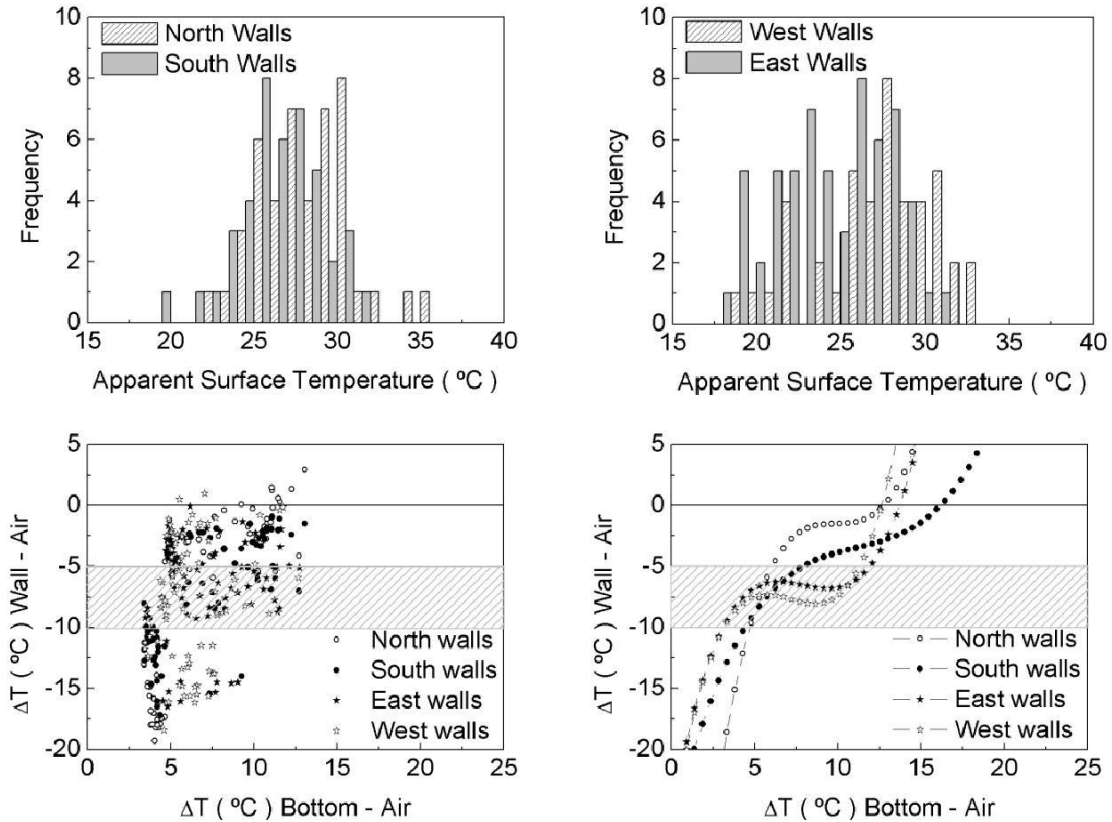


**Figure 12.** Sampling distribution of the apparent temperature of the walls, to the canyons positioned toward zonal (above, left) or in the meridional direction (above, right). Distribution of thermal amplitude between the walls and the air relative to the temperature range of the canyon floor and the air (below, left), suggesting the profiles that best fit polynomial to these distributions (below, right). The walls cardinal distribution is referenced by an imaginary observer positioned inside the building, which sees beyond the windows. The hatched areas (below) represent the range where prevail mixed scenes between walls and sky.

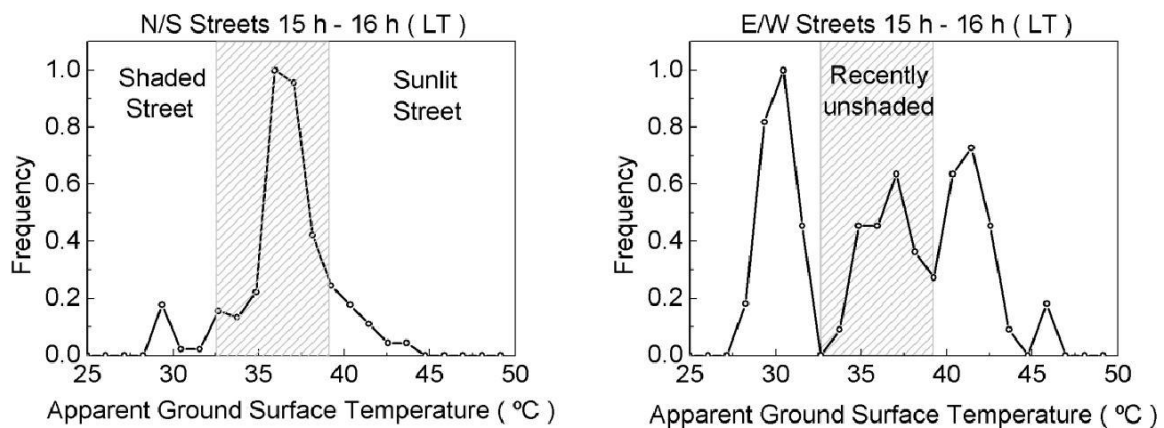


**Figure 13.** Sampling distribution of the apparent temperature on the meridional (left) and zonal (right) canyons floor.

the apparent wall temperatures have a vertical distribution and tend to have lower values for angles of elevation around 45° (Figure 11, bottom left).

**Classification**

Spatial distribution was classified according to the type of

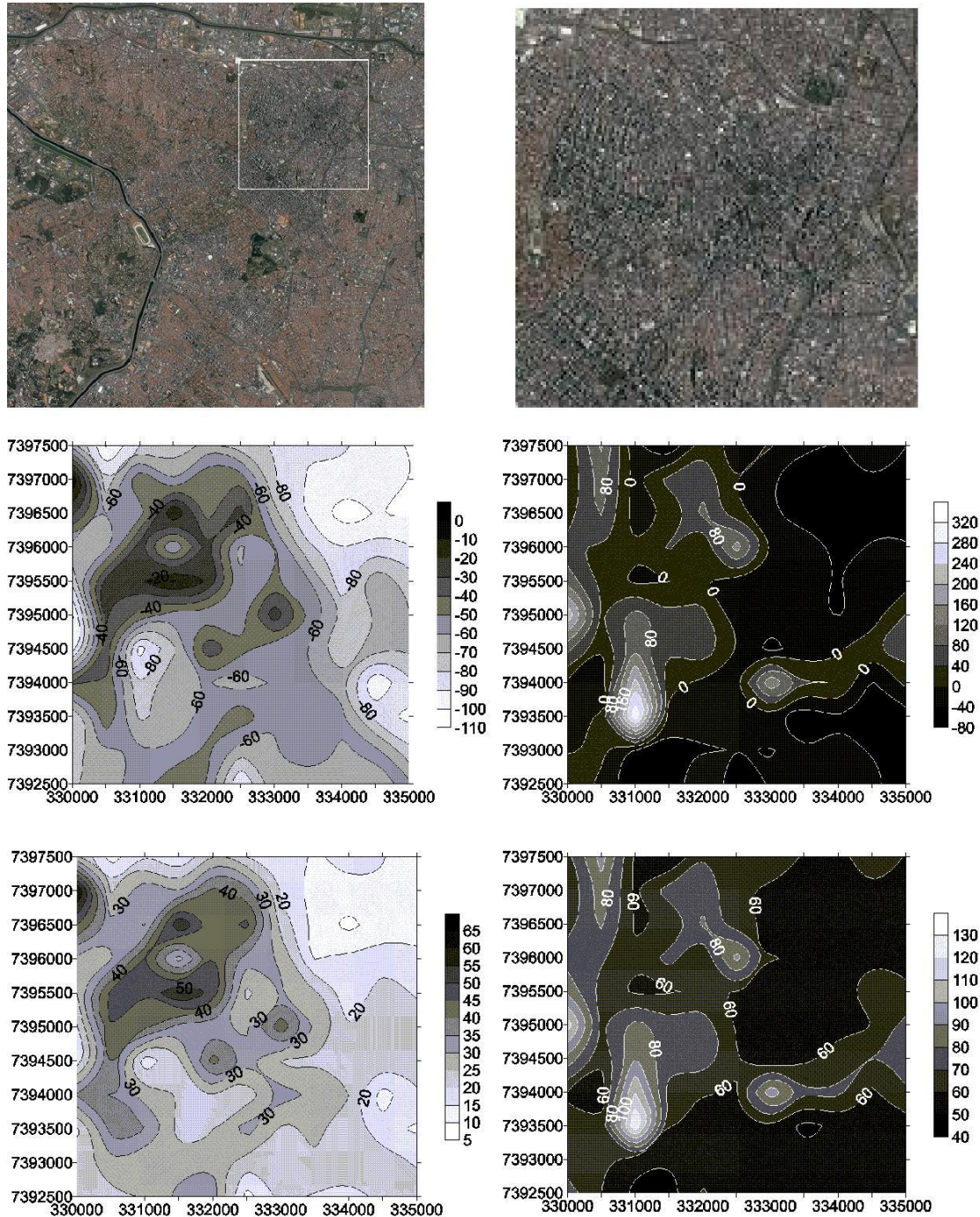


**Figure 14.** SPOT image of São Paulo (above, left). The white polygon delineates the downtown area (above, right). Spatial distribution of  $L^*$  (center, left),  $Q^*$  (center, right) and  $Q_H$  (below, left) fluxes in  $Wm^{-2}$ , and the estimated vapor pressure (below, right) in hPa.

urban land cover and land use. Four characteristic types of land use with their respective cover were identified: areas with mainly vertical surfaces (Figure 14), predominantly green areas (Figure 15), areas where the predominant buildings were factories and warehouses beside broad avenues and, lastly, residential areas where

low buildings with up to three floors interspersed with occasional taller buildings predominated.

Based on the distributions identified, the radiative fluxes were characterized in terms of the four types of surface chosen as being representative of the variety of urban land use and cover in the SPMR (Table 5)

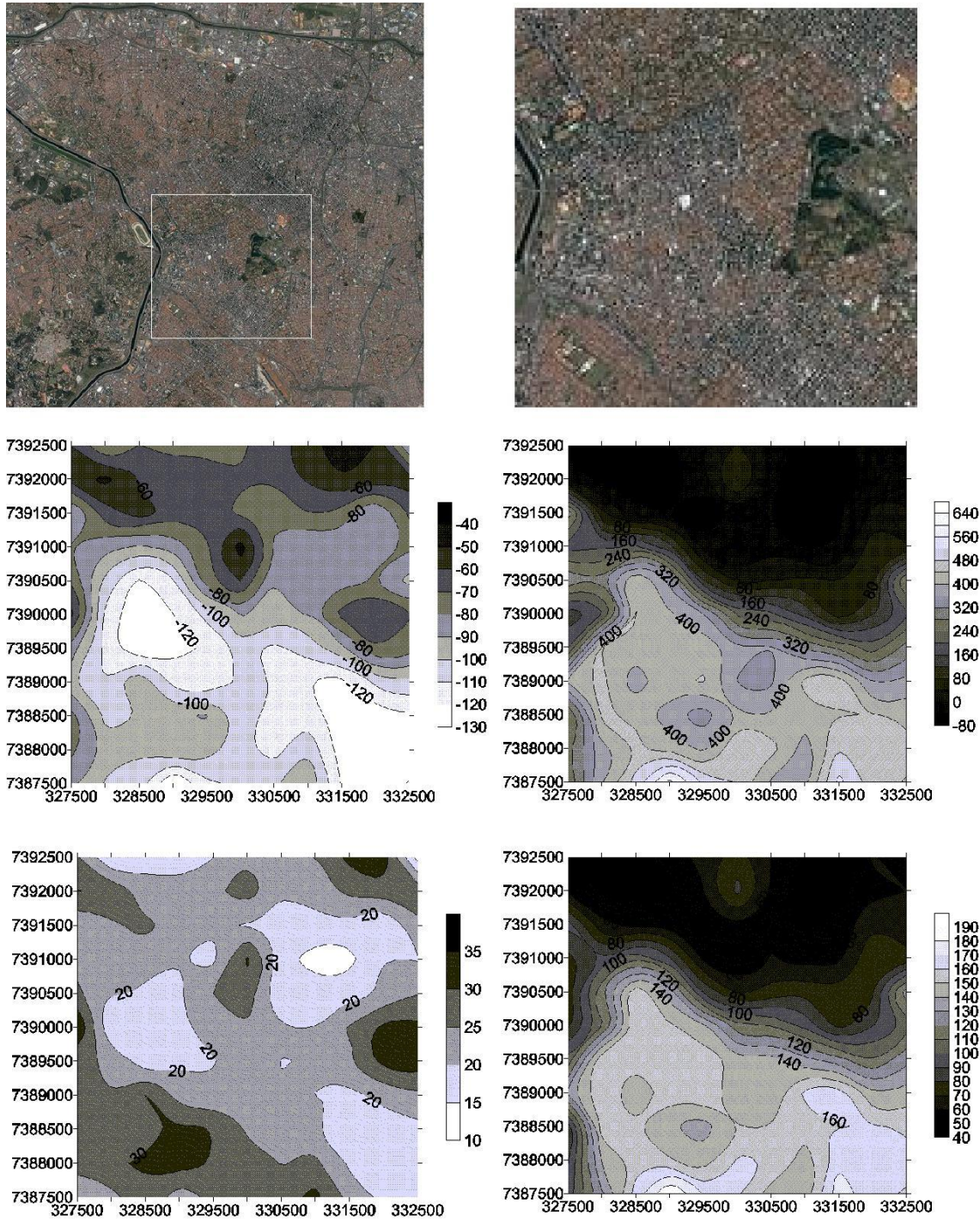


Figure 15. Same as Figure 14 for green neighborhoods of São Paulo, from the Ibirapuera Park and Gardens to the floodplain of the Pinheiros river.

## DISCUSSION

### The impact of temporal issues on mobile observations

The response-time problem inherent to each sensor has

yet to be fully understood. Table 1 shows the response time of each instrument. An extremely short sampling interval was used (2 s) to take advantage of the fast response time of the pyrgeometer and IRT sensors. However, this implies that the signal corresponding to  $Q^*$  becomes less important since the net radiometer has a

**Table 5.** Spatially averaged fluxes of  $L^*$  (longwave),  $Q^*$  (net all-wave) and  $K^*$  (shortwave) observed and estimated over different types of land use. The obtained values are associated with their respective relative errors.

Fluxes	Vertical	Green	Industrial	Residential
$L^*_M$ ( $Wm^{-2}$ )	-56.9	- 79.3	-79.3	- 33.3
$L^*_{RE}$	0.7 (1.2%)	1.8 (2.3%)	0.9 (1.1%)	2.8(8.4%)
$Q^*_M$ ( $Wm^{-2}$ )	- 0.7	137.7	72.1	73.0
$Q^*_{RE}$	2.1 (300.0%)	14.1 (10.2%)	5.4 (7.5%)	13.4(18.4%)
$K^*_M$ ( $Wm^{-2}$ )	56.2	217.0	151.4	106.3
$K^*_{RE}$	2.4 (4.3%)	15.6 (7.2%)	5.7 (3.8%)	16.0(15.1%)

longer response time (approx. 10 s). Because of this a 10 s interval was used to store the data. By using a storage interval that corresponded exactly to the response time of the net radiometer, the loss of representativeness of the  $Q^*$  signal during sampling was compensated for during data storage. In this way the data could be analyzed safe in the knowledge that they did not simply correspond to spurious values.

The first significant evidence to emerge from the systematic analysis of the data is represented clearly in Figure 4, which shows the results of three case studies on different days, sometimes at the same time, at other times not, but always along the same route. It can be seen that both flux  $L_{\downarrow}$  and temperature (especially during the day) vary by fairly large amounts for short periods of time (a few minutes). These extreme variations can only be seen in fixed observations when much longer time intervals are used (several hours). Amplitudes of  $L_{\downarrow}$  varying from 20 to 60  $Wm^{-2}$  could be observed even when mean values stored for two locations very close in time and with quite different types of cover were used. If the absolute maximum and minimum values stored were taken into account, this variability could be much higher and could reach a figure of around 80  $Wm^{-2}$ . It should be noted that only the more common patterns were considered. Extreme cases with amplitudes in excess of 100  $Wm^{-2}$  can be identified if the whole SPMR is considered, but although significant, they are less common and are therefore not discussed here.

Nevertheless, even though the variability of thermal emissions associated with  $L_{\downarrow}$  is not as great as for the flux  $L_{\uparrow}$ , it provides a good indication that the apparatus proposed here is able to recognize different patterns of thermal equilibrium in the SPMR. These patterns are less noticeable for the air temperature but follow a similar pattern even when data from different sensors are analyzed.

### Spatial distribution of long-wave emissions

Georeferencing of the data was a crucial part of the study not only because it enabled fluxes to be located geographically, but also because it allowed the spatial

distribution of those fluxes over parts of the SPMR that are very different and have very specific urban land covers to be measured exactly (Table 3 and Figure 3). At least 140 locations covering 25 different types of land use were documented in detail, and some were visited more than ten times in different weather conditions, during the day and night and at different times of the year. This observational effort resulted in an extensive data-collection grid that extended beyond the limits of the municipality of São Paulo into other neighboring urban areas in the metropolitan region. However, in general, the four elements of urban land cover that play an essential role in the fluxes observed here (trees, asphalt, walls and air) were always present in all the different areas of the SPMR investigated and only varied in the way they were distributed.

While the proposed experimental arrangement allows the vertical components of  $L^*$  (those most commonly reported in the literature) to be determined, the simultaneous use of IRT sensors on the sides of the vehicle to measure emissions from the walls allows the components of  $L^*$  parallel to the canyon floor, which are not usually reported in the literature, to be determined as well. However, inclusion of these latter emissions would significantly complicate the analysis described here, and it was therefore decided to limit the analysis to the type of investigation of fluxes normally found in the literature.

As mentioned in earlier, long-wave emissions experienced by pedestrians depend not only on the vertical balance but also on the horizontal component of emissions from walls and other vertical surfaces. For example, in a hypothetical situation in which the walls were taken into consideration, the resulting long-wave emission would be not only from the asphalt but in an oblique direction with some influence from horizontal emissions from façades. Our observations suggest that this angle of inclination with the normal to the asphalt is in the region of 15°. Consequently, the estimate of the effective urban emissivity should include, in addition to the contribution from the asphalt street cover, the contribution, albeit generic, made by walls and façades (Table 4).

In this regard, the fixed control experiments in *Rua*

*Sebastião Cortes* were extremely important and served to calibrate the mobile experiments. The temperature of the asphalt cover (Figure 10, on the left) has a frequency distribution with a very well defined maximum in the region of 22.5°C, while the distribution of the apparent wall temperature measurements (Figure 10, on the right) is bimodal, with maximum values of around 19 and 24°C. Furthermore, the distribution of apparent temperatures is more concentrated around the maximum (300 instances) than it is for the less dense distribution for the temperature of the asphalt (250 instances).

### Location of long-wave emissions

The spatial distribution for the various terms of the radiation balance at the urban surface can be determined from the data acquired for the four main types of cover observed in the SPMR (Table 5). In terms of  $Q^*$ , the green areas appear to be the main absorbers of radiative fluxes in the SPMR and can accumulate an average of more than  $130 \text{ Wm}^{-2}$ . It would seem reasonable to attribute this accumulation of energy in these parts of the city to the fact that the asphalt surface receives more diffuse solar radiation than direct radiation because of the scattering effect of the trees. As a result, less solar radiation is reflected by the asphalt, and less long-wave radiation is emitted because of the lower surface temperature. However, when the components  $L^*$  and  $K^*$  are investigated, it can be seen that long-wave emissions from the asphalt are some of the highest in these parts of the city ( $-79 \text{ Wm}^{-2}$ ), leading one to the conclusion that in general terms this surface is heated more, whether by incident solar radiation or by the friction of tires on the asphalt. However,  $K^*$  is much higher in these parts of the city (in excess of  $200 \text{ Wm}^{-2}$ ), which appears to suggest that the main factor leading to a higher  $Q^*$  in green areas is the scattering of short waves by tree foliage. Indeed, the value observed for  $Q^*$  is the same magnitude as the diffuse solar component (short waves) observed in São Paulo on overcast days in an earlier study (Ferreira et al., 2012). In other words, tree cover plays a similar role to that played by cloud cover.

Of note among the other types of cover is the balance between long waves and short waves in areas of the metropolis where there is vertical development, resulting in extremely low absolute values of  $Q^*$ , with a slight trend toward negative values. In industrial and residential areas, in contrast, intermediate values of  $Q^*$  of around  $70 \text{ Wm}^{-2}$  were observed. However, the components  $L^*$  and  $K^*$  are greater in industrial areas, probably because these contain wide avenues, as a result of which there is a greater incidence of solar radiation, the asphalt cover is heated more and, consequently, more long-wave radiation is emitted. In residential areas this effect is reduced because the form factor is generally higher. In other words, in residential areas the streets are narrower and there are occasional higher façades, so that the

streets are overshadowed more often.

### Conclusions

The method used here has made possible a number of advances in urban climatology research. The mobile observations allowed radiometric patterns to be identified below roof level, in the layer usually known as the urban canopy layer (UCL), which is far from being made up of homogeneous surfaces.

When radiative flux is defined as a characteristic of a particular area, a volume of air that fills the UCL for this area is automatically considered. Mobile observations inside this volume close to the bottom of the UCL can reveal variations in the magnitude of the radiative flux and the spatial distribution of these variations. This study therefore proposes that radiometric studies of the SPMR be reassessed as these are very often—indeed nearly always—based on data obtained from fixed observations in a single location and ignore the great variability of urban land cover and, hence, local climates in this study area.

Identification of the patterns reported here was only made possible by continual mobile observations and high-frequency acquisition of data. It is highly unlikely—indeed almost impossible—that these patterns could be identified using a network of fixed observation points, as the spatial details associated with the variability of radiative fluxes at both the local-climate and mesoclimate level can only be identified by a moving observer. Unlike convective fluxes, where an observer cannot be certain that the effect is primarily local or due to advection, in the case of radiative fluxes this possibility does not exist.

Mobile observations inside the UCL are more realistic and can be used to improve and calibrate estimates of radiative flux made from orbital platforms. The results obtained by simultaneously using a net radiometer and IRT sensors on the front and sides of the vehicle, respectively, suggest that improvements need to be made to the geometric corrections applied to data from satellite images for the purposes of analyzing urban form. Furthermore, the many different types of land use encountered mean that there is a great variety of materials, which also influences the analysis of form and its properties.

The novel use of a net radiometer in these experiments should also be emphasized, as rather than being merely an uncommon observational tool used in a different way, this device made possible two advances in the study of urban climate in the lower portion of the UCL. Firstly, as was shown, the use of a net radiometer with a pyrgeometer allowed a complete estimate of long-wave radiative flux to be made, including  $L^*$  and the component emitted by asphalt ( $L\uparrow$ ). Secondly, when used with an automatic datalogger, which allows the sampled data to be viewed in real time, the researcher has a unique opportunity to observe the spatial variations in radiation

associated with the various climate sensations he experiences in different urban areas.

The authors support the fact that much research need to be done to improve the observations and undertake more in-depth analysis as other sensors are added to the mobile platform. Clearly, the use of a humidity sensor on the proposed platform would provide a picture of the spatial distribution of humidity. Water can be expected to play an important role in urban surfaces as an emitter of long waves, particularly in tropical cities. If humidity were included in the analysis, the spatial distribution of important parameters associated with urban climate, such as the Bowen ratio, could be determined. Furthermore, although there are various issues concerning their use on mobile platforms, the use of turbulence sensors could be a bold step towards gaining a better understanding of how energy is shared between the different terms of the energy balance equation that can be observed inside the UCL.

## ACKNOWLEDGMENTS

The authors would like to thank the *Fundação de Amparo à Pesquisa do Estado de São Paulo* (FAPESP) for providing financial support (ref. no. 2005/56287-0) and the *Conselho Nacional de Desenvolvimento Científico e Tecnológico* (CNPq-Brazil) for providing a doctoral scholarship (ref. no. 141746/2006-8). They would also like to express their gratitude to the anonymous reviewers, whose comments have helped improve this paper, and Professor Colin Richard Bowles for his valuable assistance.

## Symbol

$G^D$  : Generic flux of energy over a diverse field ( $W m^{-2}$ );  
 $G_i$  : Generic flux of energy on a unit-specific domain ( $W m^{-2}$ );  
 $K_{\downarrow}$  : Incoming shortwave radiation at the surface ( $W m^{-2}$ );  $K_{\uparrow}$  : Outgoing shortwave radiation at the surface ( $W m^{-2}$ );  $K^*$  : Net shortwave radiation at the surface ( $W m^{-2}$ );  
 $L_{\downarrow}$  : Incoming longwave radiation at the surface ( $W m^{-2}$ );  $L_{\uparrow}$  : Outgoing longwave radiation at the surface ( $W m^{-2}$ );  $L^*$  : Net longwave radiation at the surface ( $W m^{-2}$ );  
 $Q^*$  : Net all-wave radiation at the surface ( $W m^{-2}$ );  $Q_E$  : Latent heat flux ( $W m^{-2}$ );  
 $Q_F$  : Anthropogenic energy flux ( $W m^{-2}$ );  $Q_H$  : Sensible heat flux ( $W m^{-2}$ );  
 $a_i$  : An unit area of the domain ( $m^2$ );  
 $\Delta Q_A$  : Net energy (sensible and latent) advection ( $W m^{-2}$ );  
 $\Delta Q_S$  : Net stored energy in the canopy (road, walls, roof and air inside the building ( $W m^{-2}$ ).

## REFERENCES

- Bárbaro E, Oliveira AP, Soares J, Codato G, Ferreira MJ, Mlakar P, Božnar MZ, Escobedo FJ (2010). Observational characterization of the downward atmospheric longwave radiation at the surface in the city of São Paulo. *J. Appl. Meteorol. Climatol.*, 49(12): 2574-2590.
- CETESB – *Companhia de Tecnologia e Saneamento Ambiental do Estado de São Paulo* (2009). (in Portuguese) <http://www.cetesb.sp.gov.br/ar/qualidade-do-ar/31-publicacoes-e-relatorios>
- Ferreira MJ, Oliveira AP, Soares J, Codato G, Bárbaro EW, Escobedo JF (2012). Radiation balance at the surface in the city of São Paulo, Brazil: diurnal and seasonal variations. *Theoret. Appl. Climatol.*, 107: 229-246.
- Ferreira MJ, Oliveira AP, Soares J (2013). Diurnal variation in stored energy flux in São Paulo city, Brazil. *Urban Clim.*, 5: 36-51.
- Hu Z, Islam S, Jiang L (1999). Approaches for aggregating heterogeneous surface parameters and fluxes for mesoscale and climate models. *Boundary-Layer Meteorol.*, 93: 313-336.
- Krayenhoff ES, Christen A, Martilli A, Oke TR (2013). A multi-layer radiation model for urban neighbourhoods with trees. March 2013. *Urban Clim. News*, pp. 7-11.
- Loridan T, Lindberg F, Jorba O, Kotthaus S, Clarke SG, Grimmond CSB (2013). High resolution simulation of the variability of surface energy balance fluxes across central London with urban zones for energy partitioning. *Boundary-Layer Meteorol.*, 147(3): 493-523.
- Machado AJ, Azevedo TR (2007). Detection of the urban heat-island effect from a surface mobile platform. *Revista de Teledetecção*, 27: 59-70.
- Machado AJ (2009). *Distribuição espacial do fluxo radiativo em ondas longas na Região Metropolitana de São Paulo*. D.Sc. Thesis. São Paulo: University of São Paulo, 295pp. (in Portuguese). <http://www.teses.usp.br/teses/disponiveis/8/8135/tde-04122009-163851/pt-br.php>
- Machado AJ (2012). Net all-wave radiation in the city of São Paulo, Brazil. *In: 8<sup>th</sup> international conference on urban climate – ICUC8*, 6<sup>th</sup>-10<sup>th</sup> August 2012, Dublin, Ireland.
- Marciotto ER, Oliveira AP, Hanna SR (2010). Modeling study of the aspect ratio influence on urban canopy energy fluxes with a modified wall-canyon energy budget scheme. *Build. Environ.*, 45: 2497-2505.
- Offerle B, Grimmond CSB, Oke TR (2003). Parameterization of net all-wave radiation for urban areas. *J. Appl. Meteorol.*, 42: 1157-1173.
- Offerle B, Grimmond CSB, Fortuniak K, Klysiak K, Oke TR (2006). Temporal variations in heat fluxes over a northern European city centre. *Theoret. Appl. Climatol.*, 84: 103-115.
- Oke TR (1987). *Boundary Layer Climates*. London, Routledge, 2<sup>nd</sup> ed.
- Soux A, Voogt JA, Oke TR (2004) A model to calculate what a remote sensor 'sees' of an urban surface. *Boundary-Layer Meteorol.*, 111(1): 109-132.

Spronken-Smith RA, Oke TR, Lowry WP (2000) Advection and the surface energy balance of an irrigated urban park. *Int. J. Climatol.*, 20: 1033-1047.

Stewart I (2011). A systematic review and scientific critique of methodology in modern urban heat island literature. *Int. J. Climatol.*, 31: 200-217.

Voogt JA, Oke TR (1998). Radiometric temperatures of urban canyon walls obtained from vehicle traverses. *Theoret. Appl. Climatol.*, 60: 199-217.